A distributed resistance analogy for solid oxide fuel cells

Beale, Steven B.; Zhubrin, Sergei V.

Publisher's version / Version de l'éditeur:

CHT-04 - Advances in Computational Heat Transfer III. Proceedings of the Third International Symposium, on board MS Midnatsol, Norwegian Coastal Voyage, 19 - 24 April, 2004, CHT-04-125, pp. 1-17, 2004

NRC Publications Record / Notice d'Archives des publications de CNRC:
https://nrc-publications.canada.ca/eng/view/object/?id=72f800ad-ccf0-438e-a111-93a5c6e54d43
https://publications-cnrc.canada.ca/fra/voir/objet/?id=72f800ad-ccf0-438e-a111-93a5c6e54d43

Proceedings of CHT-04
ICHMT International Symposium on Advances in Computational Heat Transfer

April 19-24, 2004, Norway

CHT-04-125

A DISTRIBUTED RESISTANCE ANALOGY FOR SOLID OXIDE FUEL CELLS

Steven. B. Beale*, Sergei V. Zhubrin**
*National Research Council
Montreal Road, Ottawa, Ontario, K1A 0R6, Canada
**Flowsolve Ltd.,
130 Arthur Road, London SW19 8AA, United Kingdom
*Correspondence author. Fax: +613 941 1571 Email: steven.beale@nrc.ca

ABSTRACT This paper describes the theory and application of the method of distributed resistances to calculations of fluid flow, heat/mass transfer and electrochemistry in solid oxide fuel cells. It is postulated that the transport equations may be simplified, by replacing diffusion fluxes with rate terms involving resistance (conductance) terms. Mass transfer effects are accounted-for by incorporating the solution to the one-dimensional convection-diffusion problem when computing inter-phase heat transfer coefficients and the Nernst potential, where wall mass fractions are required. Calculations are performed for a single fuel cell, and for a manifold-stack assembly of 10 such cells. The domain is discretised using a multiply shared space method. Both potentiostatic and galvanostatic conditions are considered. Calculations performed using the distributed resistance analogy, are compared to those obtained using a detailed numerical method whereby the full transport equations are solved on a fine mesh. Agreement is excellent. It is concluded that the distributed resistance analogy may be used to successfully predict transport phenomena in fuel stacks at a fraction of the computational cost required to perform calculations using conventional means.

INTRODUCTION

Distributed resistance analogy The distributed resistance analogy was first introduced by Patankar and Spalding [1] in the context of heat exchanger design. The basic problem was one of scale: namely that it was not possible, at the time, to discretise an entire heat exchanger containing numerous tubes, sufficiently fine enough to capture the detailed flow around each individual tube on the shell-side, due to the large requirements for computer memory. Figure 1 is a schematic of one such heat exchanger. The solution proposed by the authors, was to prescribe the resistance, F, and heat transfer coefficients, α, for the tubes in the bank, but still solve for the superficial flow around the baffles. The authors referred to this local-volume-averaging technique, as a distributed resistance analogy (DRA). Values of the drag coefficient, f, and the Nusselt number, Nu, may be obtained either by performing experiments, or from closed-form mathematical analysis, or by performing detailed numerical simulations for single tubes under periodic boundary conditions [2]. It is thus possible to perform calculations for the overall flow around the baffles, and the inter-fluid heat transfer, Fig.1(b), providing information about the equipment performance, which could not reliably be obtained using traditional 'presumed flow' analyses. More than a quarter century later, and in spite of the vastly superior memory and speed available in computers today, the problem still remains the same; and this methodology has been adopted as a design tool by some heat exchanger manufacturers.

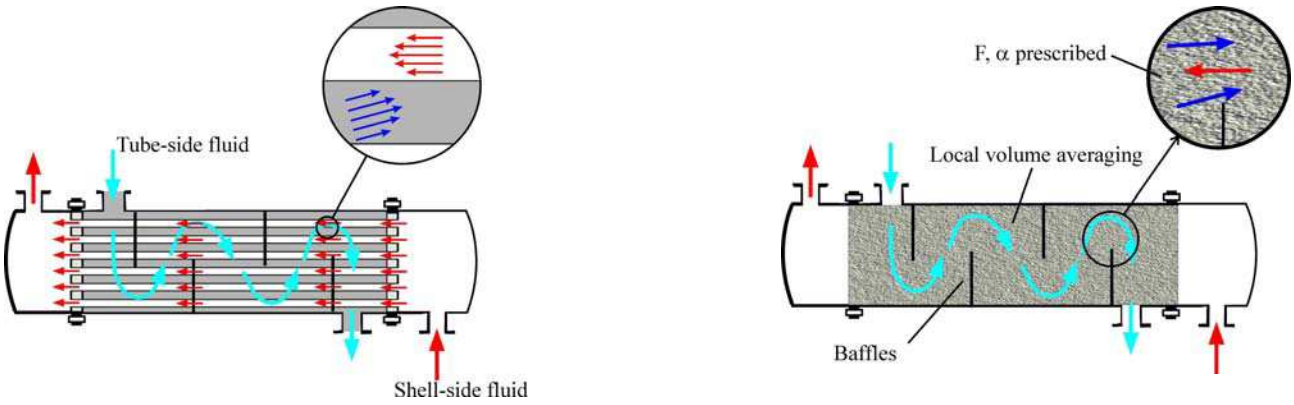

Figure 1. Shell-and-tube heat exchanger illustrating the distributed resistance analogy concept.

The original problem considered by Patankar and Spalding [1] required only the shell-side flow field be estimated; it being presumed that the tube-side flow field is sufficiently uniform, so as not to require calculation. However for many problems it is necessary that flow-field calculations be performed, simultaneously for both working fluids. A problem then arises with conventional computational fluid dynamics (CFD) codes, that while algorithms exist for performing flow field calculations for two or more distinct 'phases', generally speaking these only admit to a single value for pressure, p, at any given location. (Though in some problems, a second-phase pressure is defined which is a simple algebraic function of the regular pressure). In general then to solve flow-field problems where multiple yet distinct fluids are present, some special techniques is required. To this end, the Multiply-shared Space method (MUSES), described further below was developed.

Solid Oxide Fuel Cell The solid oxide fuel cell (SOFC) is a solid-state energy conversion device which converts chemical energy to electricity and heat. The basic components of the SOFC are the anode, cathode, and electrolyte. The electrolyte is typically Ytria stabilised Zirconia (YSZ) which allows O^{2-} ions produced at the cathode, to pass to the anode where they combine with negative electrons and fuel, presumed to be H_2, to form H_2O. SOFC's offer several potential advantages over other fuel cells, for example: A variety of fuels other than H_2, such as CH_4, may be used; The electrode-electrolyte assembly does not need to be humidified to function as a charge carrier, as in proton exchange membrane fuel cells (PEMFC's); The presence of trace elements which can 'poison' other fuel cell devices are generally not a major problem in SOFC design. However, as a high temperature device, operating in the range 800 to 1 000 °C, a new set of problems arise; specifically the mechanical integrity of the design due thermally induced stresses, as well as the temperature dependence of the performance of the cell.

Fuel cells are typically stacked together to increase the overall voltage; Figure 2 shows one such configuration. Fuel and air are introduced through manifolds at the sides of the stack. The assembly is electrically in series but hydraulically in parallel. Metallic interconnects, typically made out of stainless steel, are used to effect the electrical connection, and also serve as a housing for the air and fuel channels. Uniformity of the flow field and pressure distributions is of paramount concern in stack design.

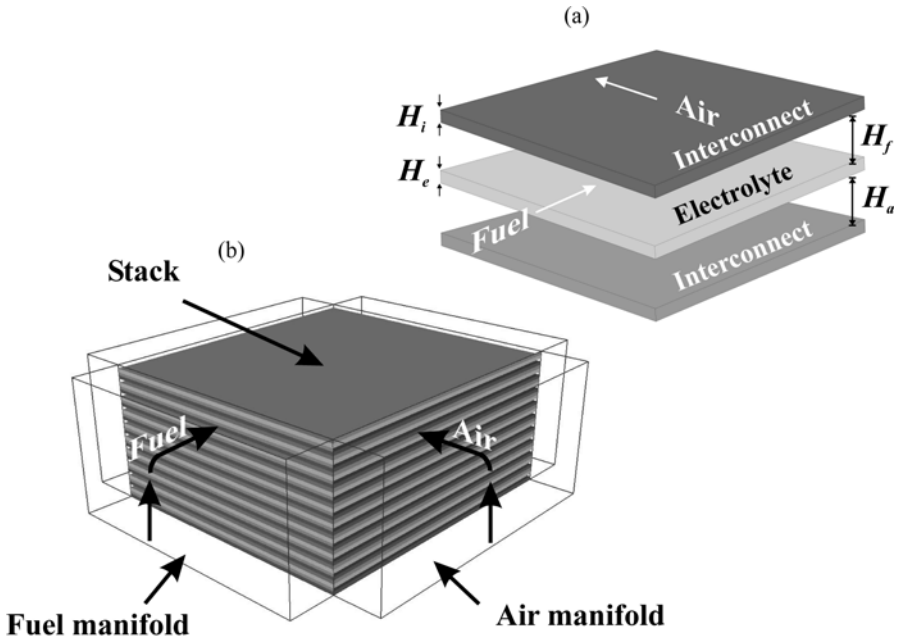

Figure 2. Schematic of fuel cell/stack geometry

Electrochemical performance. It can be shown that the ideal, or Nernst potential, E, is given by

$$E = E^0 + \frac{RT}{2F}\ln\left(\frac{x_{H_2} x_{O_2}^{0.5}}{x_{H_2O}}\right) + \frac{RT}{4F}\ln p_a \qquad (1)$$

where E^0 is a standard electrode potential, x is mole fraction, T is temperature, p_a is air pressure and $F = 96.52$ (Coulomb/kmol) is Faraday's constant. Whenever an actual current flows in a fuel cell, the cell potential, V, is lower than the ideal value,

$$V = E - i'' r_e - \eta_a - \eta_c = E - i'' r \qquad (2)$$

where i'' is the current density (A/m^2), η_a and η_c are anodic and cathodic 'overpotentials' associated with activation for the electrode half-reactions (kinetic rate-limiting factors), and r_e is the Ohmic resistance of the electrolyte. It is tacitly assumed that Ohmic losses in the metallic interconnects are negligibly small for the design under consideration. Generally-speaking, the activation overpotentials are computed with a Butler-Volmer equation [3]. However, for convenience in developing the present model, all overpotentials were lumped as a single linearised internal resistance, r, in this study [4].

PROBLEM STATEMENT

The goal of this study was to develop a simplified CFD model for an industrial SOFC design. Previous DRA studies on SOFC's involved prediction of the flow-fields only [5], and, more recently the cell/stack temperature assuming a uniform heat source corresponding to an idealised case [6,7]. This paper is the first publication where the entire electrochemical process, including non-uniform heat generation and mass transfer are considered. A detailed numerical model (DNM) was used to validate the DRA, in the absence of high quality experimental data.

The fuel cell is treated as a sandwich of four distinct materials; air, fuel, electrolyte (including the electrodes) and interconnect. For the process of developing the model theory, an idealised fuel cell prototype was considered where it is presumed that all fluid and solid regions are simple rectangular-shaped zones. Figure 2(a) illustrates the cell geometry. Because the length and width are long compared to the heights, H; the air and fuel passages may be treated as if they are planar ducts, simplifying the analysis, considerably.

A single-cell and a stack of ten (10) cells were considered: Figure 2(b) shows the stack geometry; air and fuel are admitted through risers or rectangular manifolds, pass across the cells in cross-flow and are then exhausted through downcomers or outlet manifolds. Fuel cells may be operated in co-flow, counter flow, or cross flow; however only the latter is considered in this study. Material properties are given in Table 1.

Basic Theory Let it be proposed that the governing equations are of the general form;

$$\underbrace{\frac{\partial(\rho_i \varepsilon_i \phi_i)}{\partial t}}_{\text{(i)}} + \underbrace{\nabla \cdot (\rho \varepsilon_i \vec{u}_i \phi_i)}_{\text{(ii)}} = \underbrace{\varepsilon_i \sum_j \alpha_{ij} (\phi_j - \phi_i)}_{\text{(iii)}} + \underbrace{\nabla \cdot (\varepsilon_i \Gamma \nabla \phi_i)}_{\text{(iv)}} + \underbrace{\varepsilon_i \dot{S}'''}_{\text{(v)}} \tag{3}$$

The terms in Eq. (3) are referred to as; (i) transient, (ii) convection, (iii) inter-phase transfer, (iv) diffusion or within phase transfer, and (v) source. The reader will note that the convention of Jacob [8] is adopted, whereby a 'dot' denotes a time derivative, and a 'dash' a space derivative. Therefore if q has units of Joules, then $\dot{q}'''$ is in W/m^3.

Continuity and momentum The continuity equation is straightforward, namely

$$\frac{\partial(\rho_i \varepsilon_i)}{\partial t} + \vec{\nabla} \cdot (\rho_i \varepsilon_i \vec{u}_i) = \varepsilon \dot{m}_i''' \tag{4}$$

Mass sources due to the electrochemical reactions are computed from Faraday's law,

$$\dot{m}_i'' = \pm \frac{M_i i''}{n_i F} \tag{5}$$

where i'' is current density, M is molecular weight, F is Faraday's constant, and n is the electron number. In the DRA these are coded as volumetric sources, $\dot{m}_i''' = \dot{m}_i'' / H_e$, where H_e is the height of the electrolyte.

The momentum equation presumed to be of the form

$$\frac{\partial(\rho_i \varepsilon_i \vec{u}_i)}{\partial t} + \vec{\nabla} \cdot (\rho_i \varepsilon_i \vec{u}_i ; \vec{u}_i) = -\varepsilon_i \vec{\nabla} p_i + F_i \varepsilon_i^2 (\vec{0} - \vec{u}_i) + \vec{\nabla} \cdot (\varepsilon_i \mu_i \vec{\nabla} \vec{u}_i) \tag{6}$$

The quantity F is a 'distributed resistance' [1], $\vec{u}$ is the local bulk interstitial velocity, (the quantity $\vec{U} = \varepsilon \vec{u}$ is the so-called superficial velocity). For fully-developed laminar duct flows with negligible mass transfer,

Table 1
Properties of SOFC materials

	Fuel	Air	Electrolyte	Interconnect
Volume fraction	**0.259**	**0.216**	**0.108**	**0.278**
Density, ρ, (kg/m^3)	**0.255**	**0.399**	**3300**	**7700**
Kinematic viscosity, ν (m^2/s)	**1.53×10^{-4}**	**1.1286×10^{-4}**	**–**	**–**
Specific heat, c_P, (J/kgK)	**1.6731×10^{3}**	**1.1283×10^{3}**	**598.1**	**450.0**
Thermal conductivity, k , (W/mK)	**0.08**	**0.0672**	**2.0**	**25**
Inlet interstitial velocity, u (m/s)	**0.572**	**1.839**	**–**	**–**
Inlet temperature, T (°C)	**702**	**639**	**–**	**–**
Inlet O_2 mass fraction, x_{O2}	**0**	**0.225**	**–**	**–**
Inlet N_2 mass fraction, x_{N2}	**0.85**	**0.775**	**–**	**–**
Inlet H_2 mass fraction, x_{H2}	**0.10**	**0**	**–**	**–**
Inlet H_2O mass faction, x_{H2O}	**0.05**	**0**	**–**	**–**

$$f^* = \frac{\tau_w}{\frac{1}{2}\rho u^2} = \frac{a}{\mathrm{Re}} \tag{7}$$

where the asterisk '*' denotes 'at zero mass transfer'. The Reynolds number, $\mathrm{Re} = D_h \rho u / \mu$, is based on a hydraulic diameter $D_h = 2H$, for planar geometry. It can readily be shown that,

$$F^* = \frac{2a}{\varepsilon}\frac{\mu}{D_h^2} \tag{8}$$

with a = 24, for plane ducts; Shah and London [9] provide empirical relationships for rectangular and other ducts, obtained by numerical means. Within the stack, the viscous terms in the fluids are discarded. In the manifolds, however these are non-zero, and it is the distributed resistance, F, that is set to zero.

Heat transfer The energy equation may be written in the form,

$$\frac{\partial\left(\rho_i \varepsilon_i c_{p_i} t_i\right)}{\partial t} + \vec{\nabla}\cdot\left(\rho_i \varepsilon_i \vec{u}_i T_i\right) = \varepsilon_i \sum_j \alpha_{ij}\left(T_j - T_i\right) + \vec{\nabla}\cdot\left(\varepsilon_i k \vec{\nabla} T\right) + \varepsilon_i \dot{q}''' \tag{9}$$

<u>*Source terms*</u>. Heat sources occur due to Joule heating in the electrolyte, and at the anode because of the Peltier effect. The Joule heating term is given by,

$$\dot{q}''' = i'''\left(E - V\right) \tag{10}$$

where $i''' = i''/H_e$ is the current density per unit volume (A/m^3). Peltier heating is due to the fact that the Gibbs energy does not equate to the enthalpy of formation, and must therefore be dissipated as heat in the anode; i.e. $\dot{q}'' = i''\left(\Delta G - \Delta H\right)/2F$. For the purpose of model development, no distinction between volumetric and area source terms was made, i.e., the two terms were combined as a single volumetric term.

Inter-phase heat transfer. Both terms (iii) or (iv) in Eq. (9) are present. The volumetric heat transfer coefficients are computed as

$$\alpha V = UA \tag{11}$$

where A is the area for heat transfer, V is cell volume, and U is an overall heat transfer coefficient, obtained using harmonic averaging, for example;

$$\frac{1}{UA} = \frac{1}{hA} + \frac{H}{kAS} \tag{12}$$

where S is a conduction shape factor; with S = 1 for planar geometry, A is the maximum surface area for heat transfer and H is the thickness of the solid region. Values of the heat transfer coefficient h^* were obtained from the appropriate Nu^* correlation for planar ducts, for more complex situations, these may be obtained from numerical simulation. It is interesting to note that the term α is referred to as a 'conductance', whereas F is generally considered to be a 'resistance'.

Mass transfer Species conservation may be expressed in the form;

$$\frac{\partial(\rho\varepsilon_i m_i)}{\partial t} + \vec{\nabla}\cdot(\rho\varepsilon_i \vec{u} m_i) = \nabla\cdot(\Gamma\varepsilon_i \nabla m_i) + \varepsilon_i \vec{j}_i''' \tag{13}$$

where m_i is mass fraction of species i. There are no inter-phase mass transfer terms. Mass sources/sinks have the convective form;

$$j_i''' = \dot{m}''' m_{i,t} \tag{14}$$

where $m_{i,t}$ are mass fractions at the so-called 'transferred substance state' or 'T-state' [10]. The wall values, required for the Nernst equation, may be computed from

$$m_w = \frac{m_b + m_t B}{1 + B} \tag{15}$$

where the mass transfer driving force, B, is obtained approximately [11] as,

$$B = \exp(b) - 1 \tag{16}$$

and $b = \dot{m}''/g^*$ is a blowing parameter. Mass factions, m_i, may easily be converted to molar fractions, x_i, and vice-versa.

The impact of mass transfer on the inter-phase heat transfer terms above may be incorporated as being approximately given by;

$$\frac{h}{h^*} = \frac{b}{\exp(b) - 1} \tag{17}$$

where h^* is the heat transfer coefficient for zero mass transfer. Since the conduction term in Eq. (12) is relatively minor, the term h/h^* in Eq. (17) may reasonably be replaced by α/α^*.

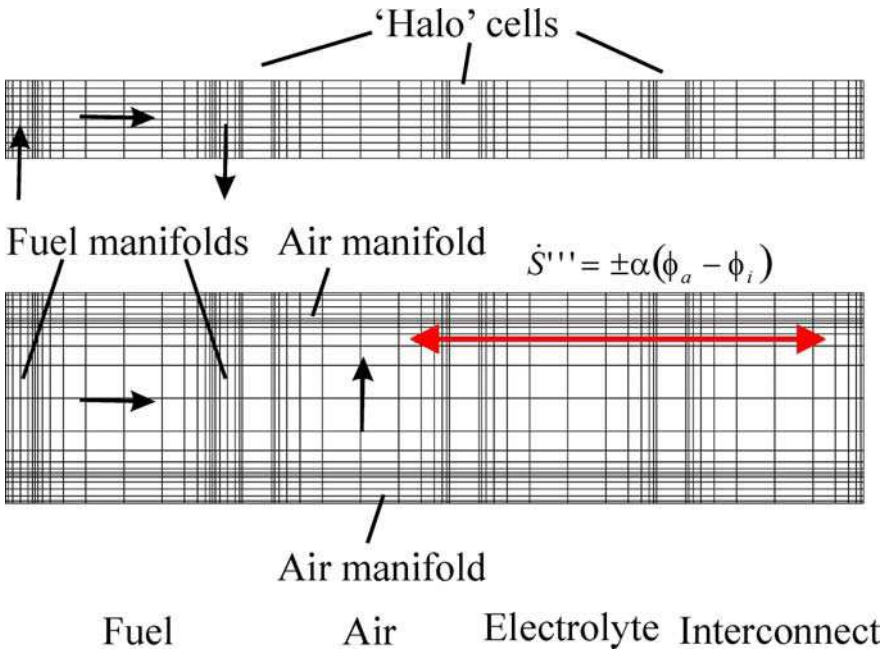

Figure 3. MUSES concept with four 'spaces': Fuel, air, electrolyte, interconnect.

Computational methodology Only steady-state cases were considered in this study and the finite-volume equations may be written [12] for a structured mesh;

$$\begin{aligned} &a_W(\phi_W - \phi_P) + a_E(\phi_E - \phi_P) + a_S(\phi_S - \phi_P) + a_N(\phi_N - \phi_P) \\ &+ a_L(\phi_L - \phi_P) + a_H(\phi_H - \phi_P) + S = 0 \end{aligned} \tag{18}$$

where *W*, *E*, *S*, *N*, *L*, *H* refer to the west, east, south, north, low, and high neighbours of cell *P*. In the present scheme, the inter-phase terms (iii) in Eq. (3) were coded in the form of linearised source terms (v) using the MUSES scheme, described further below, according to;

$$S = C(V - \phi_P) \tag{19}$$

where *C* is a source term coefficient and *V* is a source term value. Since the finite-volume equations are integrated, no distinction need be made between volumetric and area sources, viz,

$$S = \int_t \dot{S} dt = \int_t \int_V \dot{S}''' dV dt = \int_t \int_A \dot{S}'' dA dt \tag{20}$$

Multiply-shared Space method. The MUSES method was originally developed in the context of heat exchanger networks, and subsequently adapted to simultaneously model both shell and tube-side transport phenomena, and later still, solid-stresses in heat exchangers. It has also been applied to analysis of blast furnaces. Figure. 3 illustrates the fundamental mechanism of the MUSES technique as applied to the present problem: A separate space is created for each of the four component materials. For the air and fuel zones, both stack and manifolds were tessellated using a structured mesh, as illustrated in Fig. 3 (for the single cell model no manifolds are required). All redundant regions in the solids and manifolds are blocked. 'Halo' or 'ghost' cells are used to isolate the three interconnecting regions, as shown in the figure. Porosities, ε_i, are set to the values given in Table 1, except in the manifolds, where they are set to unity.

Suppose the air, fuel, electrolyte, and interconnect regions each have N_c cells in the horizontal direction and that there are N_m cells in the manifolds. Inter-phase values, *V*, for Eq. (19), for say

fuel-electrolyte pair are obtained as $V(i,j)=\phi(i\pm(N_s+1),j)$ for every (*x*,*y*) pair; a positive sign being associated with the electrolyte-to-fuel source terms and a negative sign for the fuel-to-electrolyte sources. Similarly for the air-electrolyte pair: $V(i,j)=\phi(i\pm(2N_s+N_m+2))$, the air-interconnect pair: $V(i,j)=\phi(i\pm(3N_s+N_m+3))$, fuel-interconnect $V(i,j)=\phi(i\pm(2N_s+2))$. This implementation was rendered particularly simple by employing a structured rectilinear mesh. The code used in this project was the general-purpose CFD code PHOENICS [13,14].

Computational algorithm. Let it be assumed that the following are known: Cell voltage, *V*, inlet flow rates for air and fuel, $\dot{m}_{a,i}$, $\dot{m}_{f,i}$ and mass fractions of the component species in the air $m_{\mathrm{O}_2,i}$, $m_{\mathrm{N}_2,i}$ and in the fuel $m_{\mathrm{H}_2,i}$, $m_{\mathrm{H_2O},i}$, respectively. Based on an initial guess field for *i''*, mass sources/sinks consumed/produced by the reaction, $\dot{m}_{\mathrm{O}_2}$, $\dot{m}_{\mathrm{H}_2}$, $\dot{m}_{\mathrm{H_2O}}$, are deduced from *i''* using Faraday's law. The sequence proceeds as follows;

1. Solve the transport equations
2. Solve the Nernst potential, Eq. (1) and the local current density, $i''=(E-V)/r$
3. Based on the new current density, compute values for r_e and the mass sinks/source $\dot{m}_{\mathrm{O}_2}$, $\dot{m}_{\mathrm{H}_2}$, $\dot{m}_{\mathrm{H_2O}}$, and heat source, $\dot{q}$
4. Repeat steps 1-3 until convergence is obtained.

Voltage correction. Sometimes it is convenient to prescribe the cell current, and calculate the resulting voltage (galvanostatic boundary condition); other times it is voltage which is prescribed and current which is obtained (potentiostatic boundary condition). Both situations are encountered. The above methodology is most suitable to the latter. In the galvanostatic situation, which is the *de facto* reality in stack modelling; due to the requirement that overall charge be conserved, we propose adjusting or correcting the voltage iteratively until the desired current is reached. In the approach taken here, the term $\partial V/\partial i=-r$ is computed, and the voltage adjusted from $V=V^*+\tilde{V}$, where *V** is the prescribed value of *V* at the previous iteration and $\tilde{V}$ is a voltage correction;

$$\tilde{V}=-r(\bar{i}''-\bar{i}''^*) \tag{21}$$

where $\bar{i}''$ is the desired value of the current density, and $\bar{i}''^*$ is the present value of current density (obtained by summation from local values), and *r* is an estimate of the average resistance (need not be exact).

Detailed numerical model. A previously-developed detailed numerical model [4] (DNM) was used for comparison with the model devised above. Rate equations were not assumed in the DNM rather, the diffusion terms $\Gamma\,\mathrm{grad}\,\phi$ were directly solved with a fine mesh concentrated at fluid-wall regions, as appropriate. The material and transport properties were prescribed for each region corresponding to fuel, air, electrolyte, and interconnect. Volume averaging was not therefore required.

RESULTS

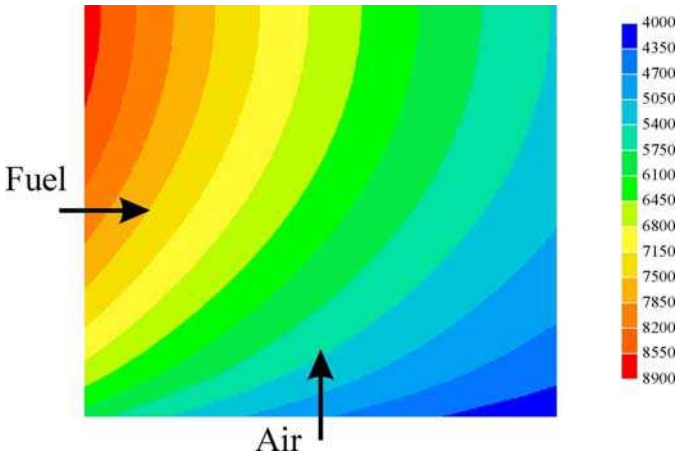

Figure 4. Current density, i'' (A/m^2), DRA, V = 0.75 V.

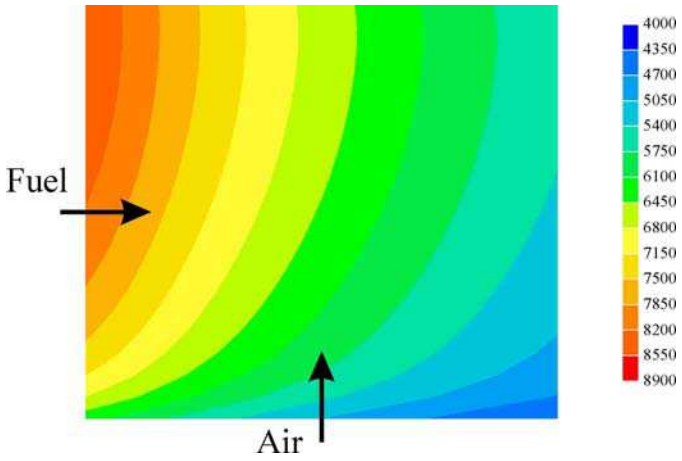

Figure 5. Current density, i'' (A/m^2), DNM, V = 0.75 V.

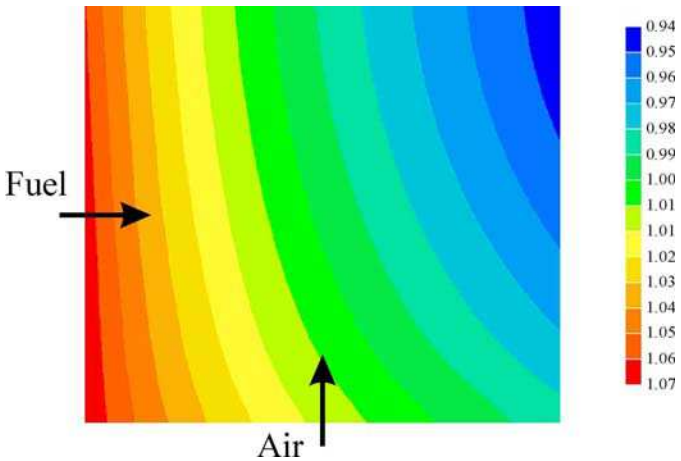

Figure 6. Nernst potential, E (V), DRA, V = 0.75 V.

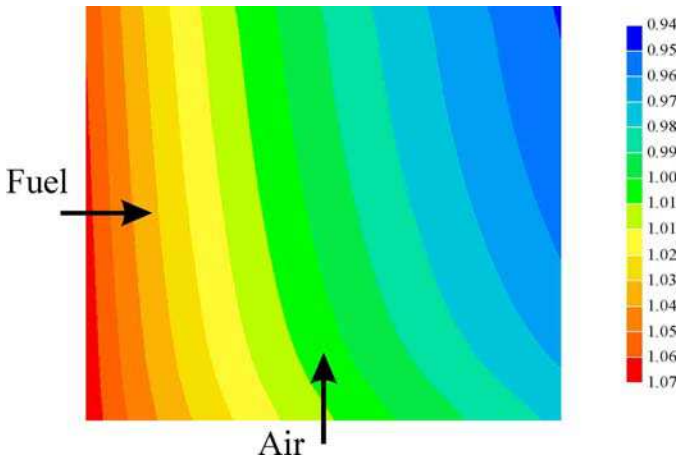

Figure 7. Nernst potential, E (V), DNM, V = 0.75 V.

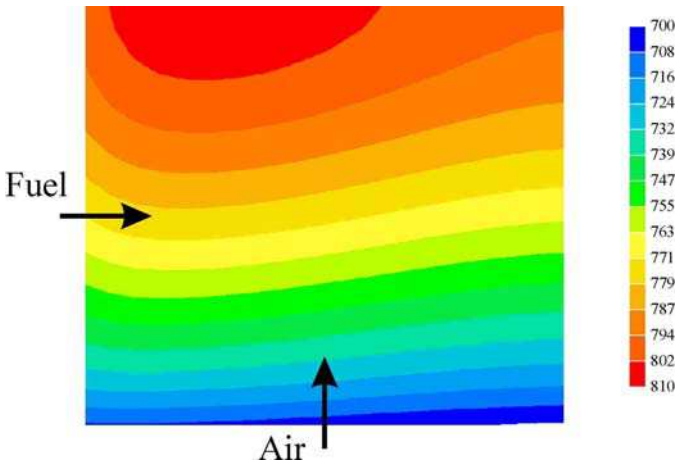

Figure 8. Temperature, T (deg. C), DRA, V = 0.75 V.

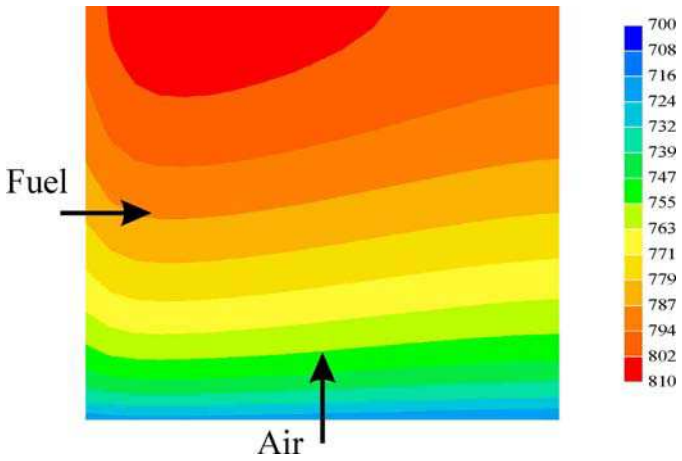

Figure 9. Temperature T (deg. C), DNM, V = 0.75 V.

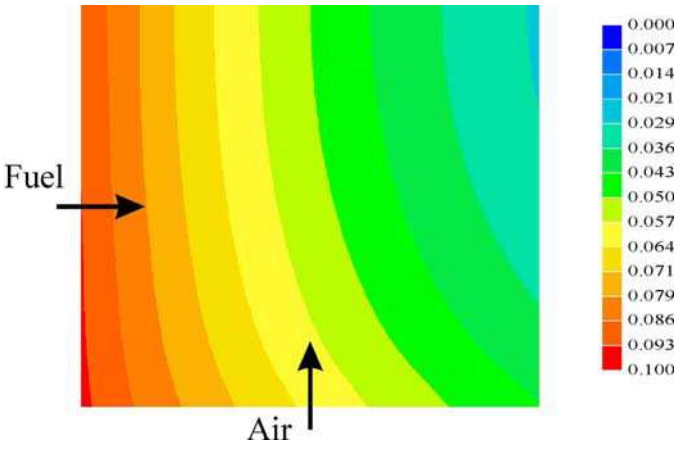

Figure 10. Anode wall H_2 mass faction, m_{H_2}, DRA, $V = 0.75$ V.

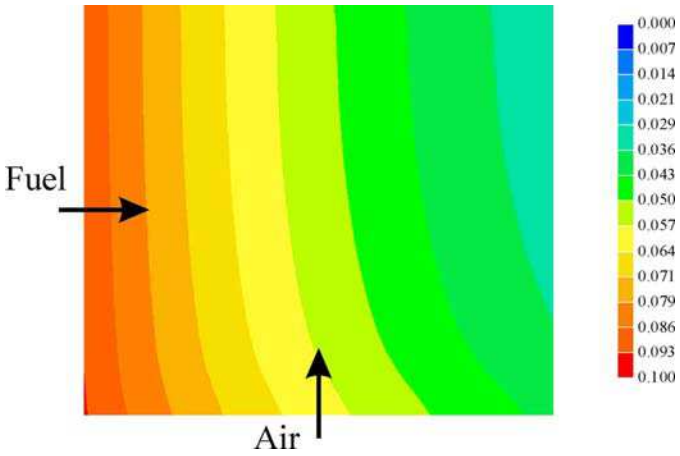

Figure 11. Anode wall H_2 mass faction, m_{H_2}, DNM, $V = 0.75$ V.

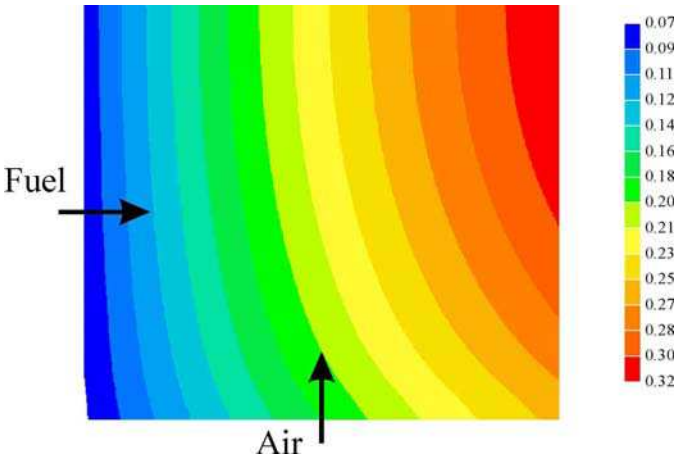

Figure 12. Anode wall H_2O mass faction, m_{H_2O}, DRA, $V = 0.75$ V.

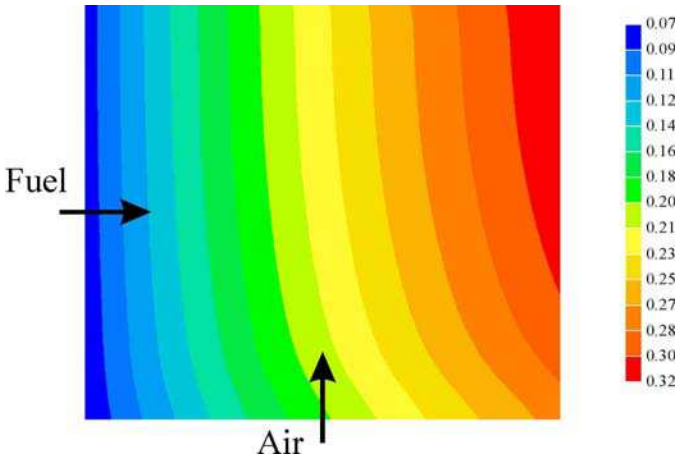

Figure 13. Anode wall H_2O mass faction, m_{H_2O}, DNM, $V = 0.75$ V.

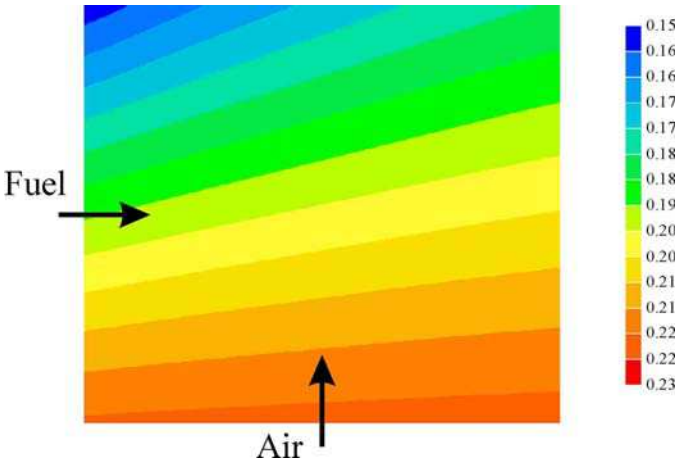

Figure 14. Cathode wall O_2 mass faction, m_{O_2}, DRA, $V = 0.75$ V.

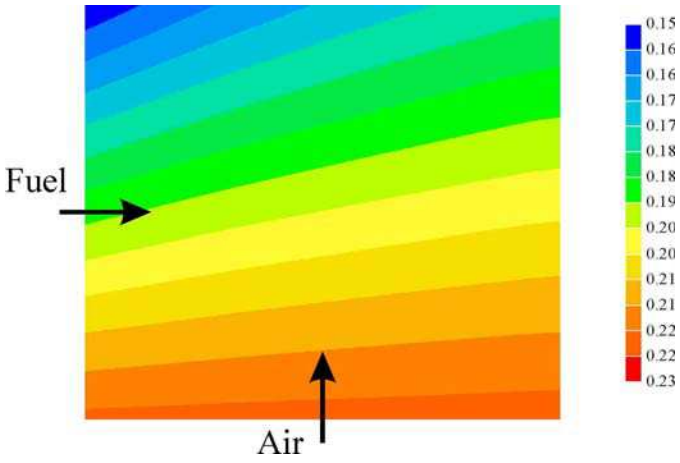

Figure 15. Cathode wall O_2 mass faction, m_{O_2}, DNM, $V = 0.75$ V.

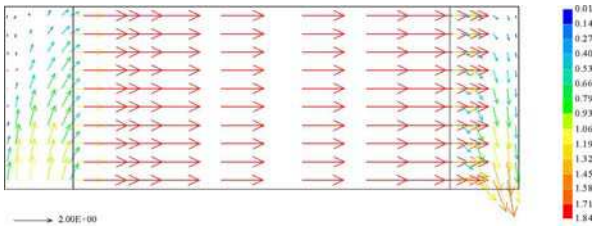

Figure 16. Air-side velocity vectors, 10-cell stack, DRA, $\bar{i}'' = 4\,000$ A/m^2.

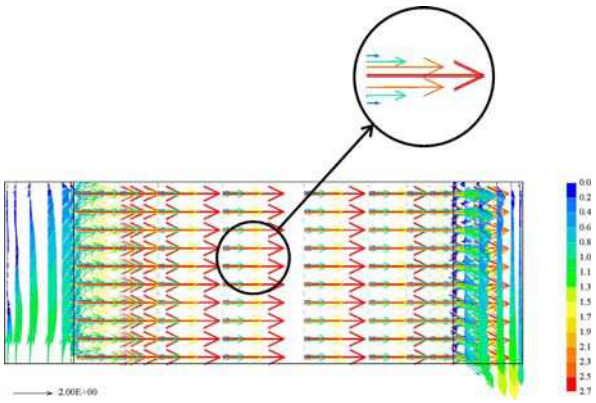

Figure 17. Air-side velocity vectors, 10-cell stack, DNM, $\bar{i}'' = 4\,000$ A/m^2.

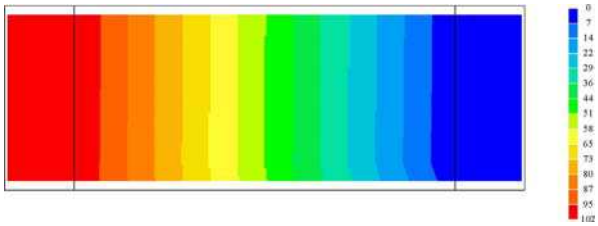

Figure 18. Air-side pressure, p_a (Pa), 10-cell stack, DRA, $\bar{i}'' = 4\,000$ A/m^2.

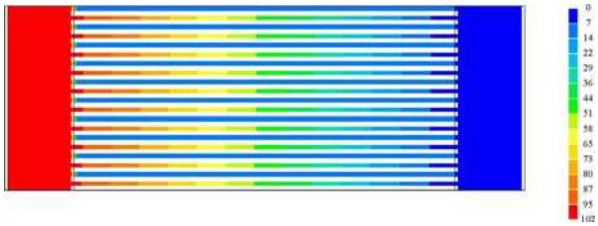

Figure 19. Air-side pressure, p, 10-cell stack, DNM, $\bar{i}'' = 4\,000$ A/m^2.

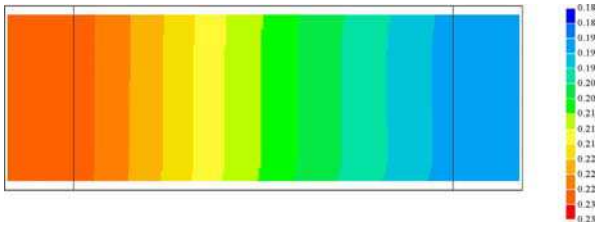

Figure 20. Air side bulk O_2 mass fraction, m_{O_2}, 10-cell stack, DRA, $\bar{i}'' = 4\,000$ A/m^2.

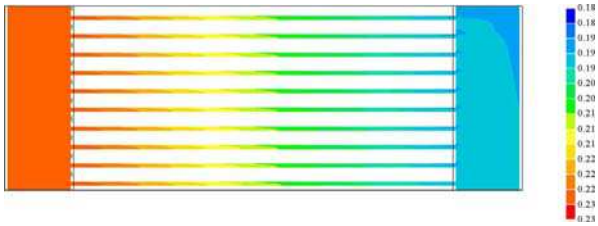

Figure 21. Air side O_2 mass fraction, m_{O_2}, 10-cell stack, DNM, $\bar{i}'' = 4\,000$ A/m^2.

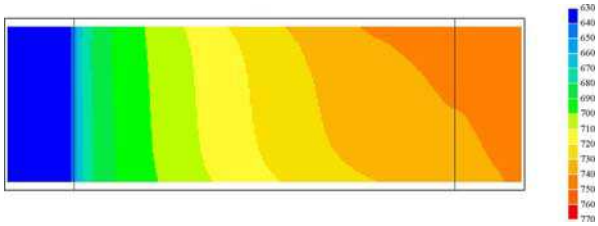

Figure 22. Air side temperature, T_a (deg. C), 10-cell stack, DRA, $\bar{i}'' = 4\,000$ A/m^2.

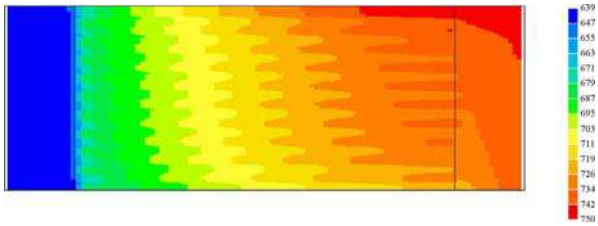

Figure 23. Temperature, T (deg. C), 10-cell stack, DNM, $\bar{i}'' = 4\,000$ A/m^2.

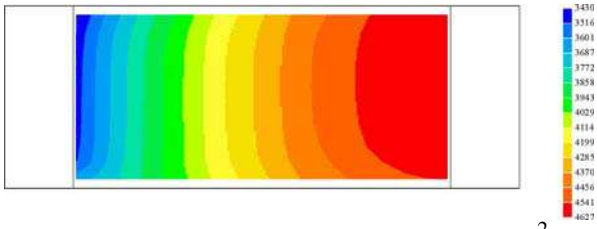

Figure 24. Current density, i'' (A/m^2), 10-cell stack, DRA $\bar{i}'' = 4\,000$ A/m^2.

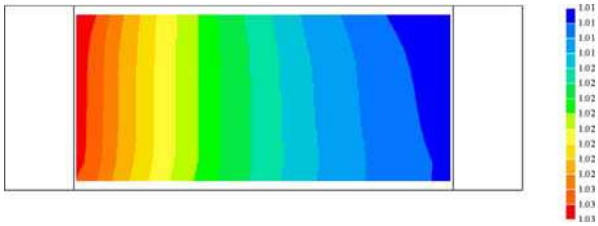

Figure 25. Nernst potential, E (V), 10-cell stack, DRA, $\bar{i}'' = 4\,000$ A/m^2.

DISCUSSION

Figures 4 to 15 are a comparison between the distributed resistance analogy and the detailed numerical method for a single cell (with no manifolds) under potentiostatic conditions with cell voltage, $V = 0.75$ V. Figures 4 and 5 show contours of current density, Figs. 6 and 7 show Nernst potential, Figs. 8 and 9 are temperature plots. Figures 10-11, 12-13 show mass fraction of H_2, and H_2O near the anode in the fuel, Figs. 14-15 are corresponding cathodic O_2 mass fractions in the air.

The H_2 contours are nominally perpendicular to, and decreasing along the fuel streamlines. A similar profile is observed for the H_2O contours, though these increase in magnitude due to the production of H_2O by the electrochemical reaction. The O_2 profile is seen to be nominally decreasing in a direction perpendicular to the O_2 flow field. Because the current density is presumed identical at the anode and cathode (for a sufficiently thin electrolyte), the source terms of H_2, H_2O and O_2 are coupled, and the mass fraction contours are skewed somewhat, this effect being more pronounced at high current densities. The Nernst potential appears to be most influenced by the H_2 and H_2O mass factions since the sum of these terms in Eq. (1) is larger in magnitude than that of the O_2 term, due to the stoichiometry of the reaction. However, E decreases as the concentrations of O_2 and H_2 are reduced and that of the H_2O increases, going from inlet to outlet, as would be expected. Both cell temperature and Nernst potential affect the current density: The temperature contours, Figs. 8 and 9, show a maximum towards the air outlet; if the power dissipated in the electrolyte were entirely uniform (constant current density and electrolyte resistance) the maximum would be at the top-right corner corresponding to the common air-fuel outlet for cross-flow. The highly conducting metallic interconnect serves as a thermal fin [6] smoothing out temperature gradients in the horizontal plane; if it were not present the difference in temperature between inlet and outlet would be much greater (a highly undesirable situation from the perspective of mechanical design). The electrolyte resistance is inversely proportional to the temperature, thus the current density increases in high temperature regions, since $i'' = (E - V)/R$. Similarly large values of the local Nernst potential will also tend to increase the local current density. Thus it is seen that there is a complex interaction between physical chemistry and transport phenomena; the subject referred to as physical-chemical hydrodynamics [15].

It can be seen that there is excellent agreement between the results of the DNM, obtained by direct solution of the finite volume equations, corresponding to the principles of balance of mass, momentum, energy and species, and the DRA which is based on the substitution of drag, heat and mass transfer coefficients (i.e. rate equations) in place of the diffusion (viscous, conduction) terms in the conservation equations. This indicates that the substitution of appropriate values for the inter-phase heat transfer coefficients and distributed resistance coefficients leads to very reasonable results at a fraction of the cost, in terms of computer time and memory. It is particularly encouraging to note that the 1-D mass transfer analysis, Eqs. (15) and (16), yields wall mass fractions of H_2, H_2O, and O_2 in close agreement with the detailed calculations since there are significant variations between m_w and m_b.

Figures 16 to 25 show sample calculations for the 10-cell manifold stack assembly, obtained for galvanostatic conditions with a mean current density of $\bar{i}'' = 4\,000$ A/m^2. Figures 16 and 17 show elevation views of velocity vectors for the air-side flow field at the centre of the stack based on calculations obtained using the DRA and the DNM methods. Figures 18 and 19 show the associated pressure distributions, Figures 20 and 21 are mass fraction of O_2. Figures 22 to 23 show the temperature distributions obtained for the air-space (DRA) and the entire stack (DNM). Figures 24 to 25 show the current density and Nernst potential obtained using the DRA.

Comparison of Figs. 16 to 19 reveal that; even though the fine detail of the motion is lost, realistic pressure and velocity data are obtained. Fig. 17 shows the characteristic parabolic-shaped velocity profile associated with fluid flow in planar ducts. This profile is clearly absent from the DRA vector field of Fig. 16, however the pressure fields are in close agreement. The results illustrate that the manifold-stack assembly is well designed hydraulically, as pressure and velocity fields are uniform throughout stack assembly. The paper by Beale et al. [5] contained a comparison of the DRA and DNM methodologies for a stack where the pressure and velocity distributions were non-uniform. The latter situation arises when pressure gradients in the manifolds are not small in comparison to those in the fuel cell passages. This can be a problem in large stacks, where suction/injection of fluid from the inlet/outlet manifolds into the stack results in the pressure gradient decreasing/increasing away from the inlet/exits to the manifolds. Inertial effects alone will cause the pressure gradient across the stack at the top to be less than across the bottom; resulting in variations in the flow field. This tendency can be minimised by ensuring the cell passages are small in comparison to the manifolds. Berman [16] presented an analysis appropriate to viscous flow in planar channels with injection/suction at both boundaries; Similar solutions for mass transfer at only one boundary were presented in [17,18].

The O_2 mass fractions are reasonably constant from cell-to-cell in the vertical direction, with good agreement between the two methodologies. The reader will note that values of m_{O_2} plotted in Fig. 20 are bulk values, unlike those shown in Fig. 14 which are wall values. Close inspection of Fig. 21 reveals significant variation in m_{O_2} across individual micro-channels; the gradients increase with increasing current density; the maximum current occurs for a short circuit, at which point $V \to 0$, and the so-called diffusion limit is reached, whereby mass transfer, not electrical resistance or kinetics, is the rate-limiting factor. At high current densities it is important that Eqs. (15) and (16) be invoked to avoid over-prediction of the Nernst potential which would occur if bulk values were used.

Figures 22 to 23 show temperature distribution assuming adiabatic (well insulated) thermal boundary conditions. The overall agreement between the DRA and the DNM is good. Plan views of the temperature distribution are qualitatively similar to those obtained for the single cell geometry, Figs. 8 and 9. The DNM results exhibit a characteristic 'zigzag' pattern, which has been noted in other studies, e.g. of heat exchangers [19,20]. This is due here, to the fact that the fuel, air, electrolyte and interconnect are all at slightly different temperatures. The electrolyte is always at a slightly higher temperature than both the air and fuel passages, due to Joule heating. Heat transfer from the electrode-electrolyte assembly to the bulk of the fluids is a function not only of the temperature difference and the heat transfer coefficients, α_{fe}, α_{ae}, etc., but also the thermal capacitances of the fluids $\dot{c} = \dot{m}c_p$. In general, the air and fuel passages will not be at the precisely same temperature. Because of the 'ordering of the streams' in the vertical direction in the stack assembly, there are secondary temperature gradients in the vertical direction. These are readily apparent in Fig. 22. In a previous study [6], it was shown that these occur even when the heat source term, $\dot{q}'''$, is completely uniform.

For single fuel cells it is quite possible to perform detailed CFD calculations using the DNM; and indeed a number of code vendors are offering fuel cell models to their clients as a software product. For large-scale industrial stacks, such methods cannot readily be applied at the present time, since the computing requirements far exceed what is generally available to the fuel cell manufacturer: The reader will appreciate that for the most part, fuel cells are fabricated with rectangular (rather than planar) passages, and that there will be hundreds or even thousands of these micro channels: It is necessary to mesh each micro channel with a fine scale mesh, in order to capture the diffusion terms near the air/fuel walls. This is simply not tenable at the present time using normal-sized

computers. Moreover at high current densities, where there is strong suction of oxygen from air, great care is required to concentrate the mesh. The DRA demonstrates that it is not necessary to use a detailed CFD code to obtain reliable performance calculations for SOFC's and stacks.

Convergence and numerical considerations Convergence was achieved, by-and-large, without difficulty. Spalding [21,22] notes that the DRA methodology is similar to a Eulerian two-phase flow formulation; in that in the event that inter-phase transfer dominate all other terms in the finite-volume equations, stability may be a matter for concern in the absence of a partial elimination algorithm or equivalent. Some oscillations were observed in the residual plots, though these did converge without difficulty, when relaxation was used. Coding the inter-phase transfer terms as source terms is a compromise: A fully-coupled solver would speed up the convergence times, compared to the segregated scheme employed here; however the MUSES method allowed a physical model to be developed in a timely manner without re-writing the CFD source code.

The voltage correction algorithm converged without difficulty for the galvanostatic case, provided a reasonable initial guess is made for the cell voltage. The reader will note that if the *V-i*'' curve is linear, and the choice *r* in Eq. (21) is correct, then the correct cell value would be predicted after only one iteration: In practice though, the *V-i*'' curve is non-linear and since *r* is only an estimate of the mean cell resistance, some iteration is required. An advantage of the voltage-correction approach adopted here, is that *r* need not be exact, and by increasing/decreasing this 'resistance' over/under-relaxation may readily be facilitated. It is of course fully acceptable to compute the average resistance by integration, and obtain the voltage as a function of this and the mean current density by numerical integration. The same result will ultimately be achieved.

The reader will note that the original form of the DRA [1] required to be modified for the stack model, since otherwise secondary thermal effects are lost, due to local volume-averaging. The reader will recall that the inter-phase heat transfer terms were computed as pairs of values for example $\dot{q}_{ae}''' = -\dot{q}_{ea}''' = \alpha_{ae}\left(T_a(k) - T_e(k)\right)$ for the air-electrolyte pair, where $k = 1, 2, 3, \ldots n_z$. A similar prescription was made for the air-interconnect and fuel-interconnect pairs. For the fuel-to-electrolyte pair however the sources were computed as $\dot{q}_{fe} = \alpha_{ae}\left(T_f(k+1) - T_e(k)\right)$, $k = 2, 3, 4, \ldots n_z$ and, $\dot{q}_{ef} = \alpha_{ae}\left(T_e(k-1) - T_f(k)\right)$, $k = 1, 2, 3, \ldots n_z$-1. Since the computational cells in the *z* direction coincided with the fuel cells, $n_z = 10$: this simple modification resulted in the secondary temperature effect being recovered, as shown in Figure 22(a). A minor disadvantage of this technique is that the computational cells must therefore coincide with the actual fuel cells in the vertical direction for the methodology to succeed.

CONCLUSIONS AND FUTURE WORK

The DRA has been shown to be an effective method for prediction of transfer phenomena in solid oxide fuel cells. In addition to fluid flow, heat and mass transfer, detailed electrochemical calculations have now been performed for the first time using the DRA. The results were validated using a DNM. The main advantage of the DRA is that it allows reliable calculations to be obtained for non-uniform flow and current density fields, at a fraction of the computational cost needed to perform detailed CFD calculations. The original DRA method as applied to heat exchanger design, was modified substantially to account for concentration gradients near wall regions. This is required because the Nernst equation, Eq. (1), is based on wall values, not bulk values. The success of the DRA methodology is critically dependent on the numerical values of the distributed resistances, *F*, and overall heat transfer coefficients, α. The latter were corrected, for mass transfer effects as outlined in the paper; the former were not, as it was ascertained that the driving force for momentum transfer is much smaller than that for heat/mass transfer. Of course the rate of heat

transfer does not occur at constant temperature, nor at constant heat flux, so the choice of α is to be considered an idealisation of reality. The ability to disable the diffusion terms in some, but not all directions, allowed for heat conduction in the stainless steel interconnects in the horizontal plane to be correctly incorporated into the model.

It is maintained that the sub-grid models developed for this research programme are sufficiently detailed to characterise SOFC's for engineering purposes. However, there is substantial scope for further model development and improvement: Chemical kinetics will be accounted-for using a Butler-Volmer equation, in place of the simple lumped resistance formulation, above. The Peltier heating effect (at the anode), needs to be separated from the Joule term within the bulk of the electrolyte. Murthy and Federov [23] have shown that the neglect of thermal radiation in SOFC's can lead to substantial over-prediction of the temperature field, and it is the authors' intentions to include a radiation model in future DRA-stack codes. Some CFD codes now calculate the electric field potential in the electrolyte and metallic interconnects, in place of the one-dimensional Nernst equation. For thin electrolytes a Nernst formulation is considered perfectly adequate, however there would be no problem in solving the electric potential using the distributed resistance analogy; and this would be a natural extension to the work described in this paper: Treatment of the electric potential is essentially the same as that for temperature in the solid (interconnect and electrolyte) spaces, i.e. a set of coupled diffusion-source equations.

In most practical planar SOFC's, the fluid channels are of rectangular, rather than planar geometry, with ribbed interconnects, essentially low aspect-ratio rectangular fins. It is straightforward to compute conduction shape factors for heat transfer and electrical resistance calculations. Electrodes of finite thickness are typically in the form of porous media with an associated bulk-to-interface mass transfer driving force. In addition there usually are non-participating porous gas diffusion layers (GDL's) to assist transport of the fuel and air to the electrodes from the micro-channels. Some additional research is needed to characterise mass transfer within the gas diffusion layers and electrolytes. Following such an analysis, the DRA may readily be applied to more complex geometries; either by increasing the number of spaces in the MUSES technique to include these additional layers (GDL's, electrodes etc.), and/or by correlating mass transfer in the porous media terms of a conductance-effectiveness as a function of geometry and mass flux.

Although the SOFC geometry considered in this study had a relatively simple form, and flow fields were relatively uniform; there are many other types of fuel cell where the flow-fields are far from uniform; for example cylindrical SOFC's exist which offer certain advantages from the perspective of mechanical design. In the automobile industry, proton exchange membrane fuel cells (PEMFC's) are considered as a potential replacement for the internal combustion engine. PEMFC's are frequently designed with the flow passages in the form of serpentine-shaped channels. For such situations the DRA would prove of great utility, not only for stack-level models, but also for analysis of single cells

ACKNOWLEDGEMENTS

Dr. Wei Dong developed much of the DNM code, used to validate the DRA model, as a visiting post-doctoral fellow in the Institute of Chemical Process and Environmental Technology, at the National Research Council of Canada. Prof. D.B. Spalding contributed some useful discussion about the DRA in the early stages of the project. Mr. Ron Jerome provides technical support. The ongoing support of the NRC Hydrogen and Fuel Cells Program is acknowledged with gratitude.

NOMENCLATURE

A	Area (m^2)
a	Coefficient in finite-volume equations.
c	Thermal capacitance (J/K)
c_p	Specific heat (J/kgK)
D	Diffusion coefficient (m^2/s)
D_h	Hydraulic diameter (m)
E	Nernst potential (V)
F	Distributed resistance (kg/m^2s), Faraday's constant, 96.52 (Coulomb/kmol)
G	Gibbs free energy (J)
g	Mass transfer conductance (kg/s)
H	Height (m), enthalpy (J)
h	Heat transfer coefficient per unit area (W/m^2K)
k	Thermal conductivity (W/mK)
i	Current (A)
j	Source term in species equation (kg)
L	Length (m)
m	Mass fraction (kg/kg), mass (kg)
n	Electron number
p	Pressure (Pa)
q	Heat source term (J)
R	Gas constant (J/kgK), resistance (Ohm)
r	Resistance (Ohm/m^2)
S	Source term, conduction shape factor ( )
T	Temperature (°C)
U	Overall heat transfer coefficient per unit area (W/m^2K), superficial velocity (m/s)
u	Interstitial velocity (m/s)
V	Volume (m^3), cell potential (V)
T	Temperature (K)
x_i	Mole fraction (kmol/kg)

Greek Symbols

α	Volumetric heat transfer coefficient (W/m^3K)
ε	Volume fraction
Γ	Exchange coefficient (kg/ms)
ϕ	General scalar
η	Overpotential, polarisation (V)
ρ	Density (kg/m^3)
μ	Viscosity (W/mK)

Non-dimensional numbers

B	Driving force
b	Blowing parameter
f	Friction coefficient
Nu	Nusselt number
Sh	Sherwood number
Sc	Schmidt number
Re	Reynolds' number

Subscripts

a	Air, anode
b	Bulk
c	Cathode
e	Electrolyte
f	Fuel
i	Interconnect
t	Transferred substance state
w	Wall

Superscipts

0	Reference state
*	Zero mass transfer
'	Per unit length
''	Per unit area
'''	Per unit volume
·	Per unit time

REFERENCES

1. Patankar, S.V., and Spalding, D.B., A Calculation Procedure for the Transient and Steady-State Behaviour of Shell-and-Tube Heat Exchangers, Imperial College of Science and Technology, London, 1972.
2. Beale, S.B., and Spalding, D.B., Numerical Study of Fluid Flow and Heat Transfer in Tube Banks with Stream-Wise Periodic Boundary Conditions, *Transactions of the CSME*, Vol. 22, No. 4A, pp. 394-416, 1998.
3. Bard, A.J., and Faulkner, L.R., *Electrochemical Methods*, 2nd ed., John Wiley & Sons, New York, 2001.
4. Dong, W., Beale, S.B., and Boersma, R.J., Computational Modelling of Solid Oxide Fuel Cells, *Proceedings of the 9th Conference of the CFD Society of Canada - CFD 2001*, Waterloo, 2001, pp. 382-387.
5. Beale, S.B., Ginolin, A., Jerome, R., Perry, M., and Ghosh, D., Towards a Virtual Reality Prototype for Fuel Cells, *PHOENICS Journal of Computational Fluid Dynamics and its Applications*, Vol. 13, No. 3, pp. 287-295, 2000.
6. Beale, S.B., Zhubrin, S.V., and Dong, W., Numerical Studies of Solid-Oxide Fuel Cells, *Proceedings 12th International Heat Transfer Conference*, Grenoble France, 2002, pp. 865-870.
7. Beale, S.B., Lin, Y., Zhubrin, S.V., and Dong, W., Computer Methods for Performance Prediction in Fuel Cells, *Journal of Power Sources*, Vol. 11, No. 1-2, pp. 79-85, 2003.
8. Jacob, M., *Heat Transfer*, Wiley, New York, 1949.
9. Shah, R.K., and London, A.L. in *Advances in Heat Transfer* (ed. J. P. Hartnett) Academic Press, New York, 1978.
10. Spalding, D.B., A Standard Formulation of the Steady Convective Mass Transfer Problem, *International Journal of Heat and Mass Transfer*, Vol. 1, pp. 192-207, 1960.
11. Beale, S.B., Calculation Method for Mass Transfer in Fuel Cells, *Journal of Power Sources*, 2004.
12. Patankar, S.V., *Numerical Heat Transfer and Fluid Flow*, Hemisphere, New York, 1980.
13. Spalding, D.B., Four Lectures on the PHOENICS Code, CFD/82/5, Computational Fluid Dynamics Unit, Imperial College, University of London, 1982.
14. Spalding, D.B., PHOENICS 1984. A Multi-Dimensional Multi-Phase General-Purpose Computer Simulator for Fluid Flow, Heat Transfer and Combustion., CFD/84/18, Computational Fluid Dynamics Unit, Imperial College, University of London, London, 1984.
15. Levich, V.G., *Physicochemical Hydrodynamics*, 1962.
16. Berman, A.S., Laminar Flow in Channels with Porous Walls, *Journal of applied physics*, Vol. 24, No. 9, pp. 1232-1235, 1953.
17. Jorne, J., Mass Transfer in Laminar Flow Channel with Porous Wall, *Journal of the Electrochemical Society*, Vol. 129, No. 8, pp. 1727-1733, 1982.
18. Lessner, P., and Newman, J.S., Hydrodynamics and Mass-Transfer in a Porous-Wall Channel, *Journal Of The Electrochemical Society*, Vol. 131, No. 8, pp. 1828-1831, 1984.
19. Coelho, P.J., Mathematical Modeling of the Convection Chamber of a Utility Boiler - an Application, *Numerical Heat Transfer, Part A*, Vol. 36, pp. 411-428, 1999.
20. Coelho, P.J., Mathematical Modeling of the Convection Chamber of a Utility Boiler - the Theory, *Numerical Heat Transfer, Part A*, Vol. 36, pp. 429-447, 1999.
21. Spalding, D.B., Methods of Calculating Heat Transfer within the Passages of Heat Exchangers, HTS/81/4, Computational Fluid Dynamics Unit, Imperial College, University of London, London, 1981.
22. Spalding, D.B., The Calculation of Heat-Exchanger Performance, HTS/81/5, Computational Fluid Dynamics Unit, Imperial College, University of London, 1981.
23. Murthy, S., and Federov, A.G., Radiation Heat Transfger Analysis of the Monolith Type Solid Oxide Fuel Cell, *Journal of Power Sources*, Vol. In press, 2003.